Met. Mater. Int., Vol. 21, No. 3 (2015), pp. 470~478
doi: 10.1007/s12540-015-4421-y

Effect of Chloride Ions on the Corrosion Behavior of Low-Alloy Steel Containing Copper and Antimony in Sulfuric Acid Solution

Sun-Ah Park, Seon-Hong Kim, Yun-Ha Yoo, and Jung-Gu Kim*

Department of Advanced Materials Engineering, Sungkyunkwan University, 300 Chunchun-Dong, Jangan-Gu, Suwon 440-746, South Korea

(received date: 11 September 2014 / accepted date: 24 October 2014)

The influence of the addition of HCl on the corrosion behavior of low-alloy steel containing copper and antimony was investigated using electrochemical (potentiodynamic and potentiostatic polarization tests, and electrochemical impedance spectroscopy) and weight loss tests in a 1.6 M H_2SO_4 solution with different concentrations of hydrochloric acid (0.00, 0.08, 0.15 and 0.20 M HCl) at 60 °C. The result showed that the corrosion rate decreased with increasing HCl by the formation of protective layers. SEM, EDS and XPS examinations of the corroded surfaces after the immersion test indicated that the corrosion production layer formed in the solution containing HCl was highly comprised of metallic Cu, Cu chloride and metallic (Fe, Cu, Sb) compounds. The corrosion resistance was improved by the Cu-enriched layer, in which chloride ions are an accelerator for cupric ion reduction during copper deposition. Furthermore, cuprous and antimonious chloride species are complex salts for cuprous ions adsorbed on the surface during copper deposition.

Keywords: metals, rolling, corrosion, electrochemistry, scanning electron microscopy

1. INTRODUCTION

Increased public awareness and government efforts for a clean environment have compelled the utilities that burn sulphur-containing fossil fuel to equip flue gas desulphurization (FGD) systems [1,2]. The operation of fossil fuel power plants produces gaseous acidic substances such as SOx and Cl that cause environmental contamination. To control pollution, FGD systems were developed to remove the sulphur dioxide in the flue gas produced by coal or oil combustion. The flue gas is introduced to the FGD system through a duct, where it is absorbed and removed by chemical reactions with limestone slurry as the absorbent. However, the operating temperature of the FGD system needs to be reduced to increase the absorption efficiency of dust and sulphur compounds. When the gas temperature drops to below a dew point or the gas contacts a cold wall surface, gaseous acidic substances and H_2O in the gas combine to form a highly dilute sulfuric acid, which causes steel materials to corrode. This phenomenon is called sulfuric acid dew corrosion, which severely corrodes materials. The dew point temperature of sulfuric acid ranges from 100 °C to 150 °C, and since it differs according to the condensed sulfuric acid concentration [1-8]. It is difficult to avoid the occurrence of sulfuric acid dew corrosion in flue gas treatment facilities during operation. As these temperatures become lower, the conditions for hydrochloric acid dew corrosion by Cl^- are added to the sulfuric acid dew corrosion environment. The dew point temperature of hydrochloric acid ranges from 50 °C to 80 °C, and differs according to the condensed hydrochloric acid concentration. Therefore, the steel used requires corrosion resistance against both hydrochloric acid dew corrosion resulting from lower-temperature facilities and sulfuric acid dew corrosion [7-9].

Under these conditions, heavy corrosion occurs on ordinary steels. To solve this problem, it is important to examine the corrosion resistance of steels in sulfuric acid/hydrochloric acid environments representing FGDs. In particular, it is essential to assess low-alloy steels to develop low-cost steels with suitable corrosion resistance [3,7-9]. Since the 1930s, various studies have investigated low-alloy steels for FGD material application to reduce costs. On the basis of COR-TEN steel, POSCO developed a steel composed of C, Si, Mn, P, S, Cu, and Sb elements, called the ANCOR series, which is resistant to dew-point corrosion [1,9].

Generally, in the pitting of steels in containing chloride, a micro-environment essentially representing hydrochloric acid may be established within the pits [10,11]. It would be highly desirable to precisely image chloride concentrations at metal surfaces in chloride-containing solutions in situ, because the chloride in solution usually plays a crucial role in pitting initiation, and the chloride concentration at the interface of the

*Corresponding author: kimjg@skku.edu

metal/solution is always different from that in the bulk solution [12]. The passive film on the ferrite phase appears to be more sensitive to chloride ions [13]. Whereas, chloride ions exhibit an effect to decrease corrosion rate in a dilute sulfuric acid environment on any of the steel tested [9]. Moreover, hydrogen evolution reaction was to some extent inhibited in proportion to the concentration of the chloride ions. Note that this is expected to be the effect of the adsorption of chloride ions and the blocking of the active surface [14-16]. Therefore, previous studies about chloride ions effects have shown conflicting results.

In this study, the effect of chloride ions on the corrosion properties of low-alloy steel containing copper and antimony in highly dilute sulfuric acid solution was investigated by electrochemical tests, weight loss tests, and surface analyses.

2. EXPERIMENTAL PROCEDURES

2.1. Materials and test condition

A hot-rolled low-alloyed carbon steel sheet containing 0.07 C, 0.7 Mn, 0.01 P, 0.01 S, 0.3 Cu, 0.1 Sb and Fe balance was used in the experiments. Tensile strength, yield strength and % elongation of steel were 462 MPa, 352 MPa and 36.2%. The Steel plates, 0.35 cm in thickness, were cut into 1.5 cm by 1.5 cm specimens. The specimens were ground with 600-grit of silicon carbide (SiC) paper, cleaned with ethanol for 5 min in an ultrasonic chamber, and then dried in air.

The corrosion medium contained 1.6 M dilute sulfuric acid solution with different concentrations of hydrochloric acid (0.00, 0.08, 0.15 and 0.20 M), and was prepared by the dilution of analytical-grade sulfuric acid and hydrochloric acid in distilled water. The concentration of sulfuric acid was determined from analyses of the condensed acidic water sampled at FGD facilities in a representative heavy oil power plant in Korea. The corrosion medium was kept at 60 °C under an aerated condition throughout all the corrosion tests. The value of pH was -0.5 in all environments despite the change in concentration of hydrochloric acid.

2.2. Weight loss measurements

Weight loss measurements were performed according to the ASTM G1-90 and ASTM G31-72 standards [17,18]. The clean specimen was stored in a desiccator for 24 h before the weight loss test. After hanging the specimen with a plastic wire in a 1.6 M H_2SO_4 solution with different concentrations of hydrochloric acid (0.00, 0.08, 0.15 and 0.20 M HCl) at 60 °C for 6 h, the specimen was removed, cleaned with distilled water, and immersed in the reagents, 500 ml of a HCl solution and 3.5 g hexamethylene tetramine ($C_6H_{12}N_4$), and distilled water to make a 1000 ml solution for 5 min. The specimen was then degreased in an ultrasonic cleaner with ethanol for 5 min, cleaned with distilled water, and dried in hot air. The weight loss was then measured. At least three measurements were run for each specimen to ensure reproducibility.

2.3. Electrochemical measurements

Potentiodynamic and potentiostatic polarization tests, EIS were carried out to evaluate the corrosion behavior of the steel specimen in the dilute sulfuric acid solution with different hydrochloric acid concentrations, using a three-electrode electrochemical cell. The cell contained a steel specimen as a working electrode, a glass capillary probe connected to a saturated calomel reference electrode (SCE), and two graphite rod counter electrodes. The specimen was mounted in a cured epoxy resin, and the epoxy-specimen interface was painted, leaving an exposed area of 1 cm^2 on the material surface. The specimen was allowed to reach a stable open-circuit potential (OCP) within ± 5 mV about 20 min after immersing it in the test solution. In the potentiodynamic polarization test, the potential of the electrode was swept from a cathodic potential of -0.25 V_{OCP} to an anodic potential of about 0.25 V_{OCP} at a scan rate of 0.166 mV/s in order to obtain the Tafel slope. In the potentiostatic polarization test, a potential of -0.35 V_{SCE} was applied to the electrode for 6 h. The EIS measurements were carried out to observe the corrosion performance of the steels as a function of the immersion period. The EIS measurements were taken with an amplitude of ±10 mV over the frequency range from 100 kHz to 10 mHz. This process was repeated continuously every 1 h until 6 h. At least three measurements were run for each specimen to ensure reproducibility and then experimental data on the approximated average value were shown as a representative value.

2.4. Surface analyses

The surface properties (morphology and compositions) of the corrosion products after 6 h of immersion in a 1.6 M H_2SO_4 solution with different concentrations of hydrochloric acid (0.00, 0.08, 0.15 and 0.20 M) at 60 °C for 6 h were examined by scanning electron microscopy (SEM, S-3000H, HITACHI), energy dispersive spectroscopy (EDS, EX-220, HORIBA), electron probe X-ray microanalysis (EPMA, JXA-8900R), and X-ray photoelectron spectroscopy (XPS, SIGMA PROBE, Thermo VG, U.K). SEM was carried out at an acceleration voltage of 15 kV. EPMA was performed at an acceleration voltage of 20 kV. XPS analysis was conducted using monochromatic Al K_α radiation (15 kV). The pass energies of the wide and narrow scans were 50 eV and 20 eV, respectively.

3. RESULTS

3.1. Weight loss measurements

Figure 1 shows the corrosion rate of low-alloy steel calculated from the results of weight loss measurement after 6 h of immersion in a dilute sulfuric acid solution with various concentrations of hydrochloric acid. In the weight loss test, the corrosion rate was determined using the following Eq. [18]:

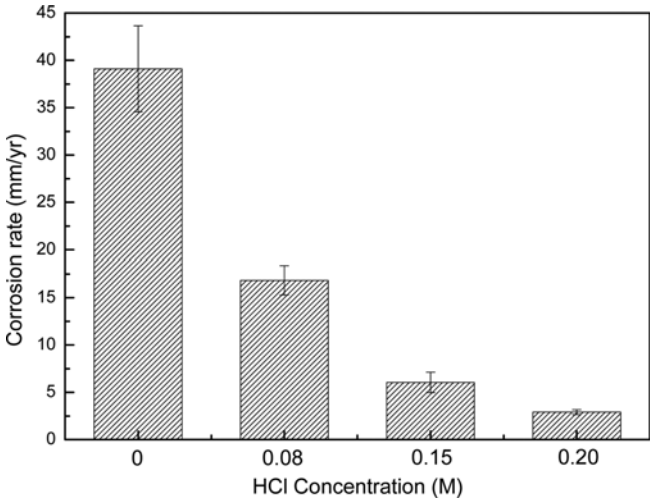

Fig. 1. Corrosion rates by weight loss measurement after 6 h of immersion in a dilute sulfuric acid solution with various concentrations of hydrochloric acid.

$$\text{Corrosion rate (mm/y)} = \frac{8.76 \times 10^4 W}{At\rho} \quad (1)$$

where 8.76×10^4 is a metric and time conversion factor, W is the weight loss (g), A is the area of exposure (cm^2), t is the exposure time (h), and ρ is the density (g/cm^3). In the absence of hydrochloric acid, the corrosion rate was relatively high (~35 mm/y). However, the corrosion rate was drastically decreased with the addition of the hydrochloric acid. In particular, the lowest corrosion rate (~3 mm/y) was observed with the addition of 0.2 M hydrochloric acid.

3.2. Potentiodynamic polarization tests

The effects of the hydrochloric acid addition with various concentrations on the corrosion behavior of low-alloy steel were examined by polarization tests. The potentiodynamic polarization tests were conducted twice for each hydrochloric acid concentration. The one was conducted after the stable open-circuit potential (OCP) of the specimen was obtained (for about 20 min), and the other did after 6 h of immersion in the solution, as shown in the polarization curves demonstrating the active anodic polarization in Fig. 2. The anodic current density was reduced due to the addition of hydrochloric acid, confirming the improved corrosion resistance by the addition of chloride ions. With hydrochloric acid added, the anodic current density after 6 h of immersion decreased compared to the anodic current density upon the initial immersion, and the corrosion potential after 6 h of immersion shifted in the noble direction compared to the corrosion potential upon the initial immersion, confirming the improved corrosion resistance by chloride ions with increasing immersion time.

The corrosion rate can be inferred from the corrosion current density based on Faraday's law [10]:

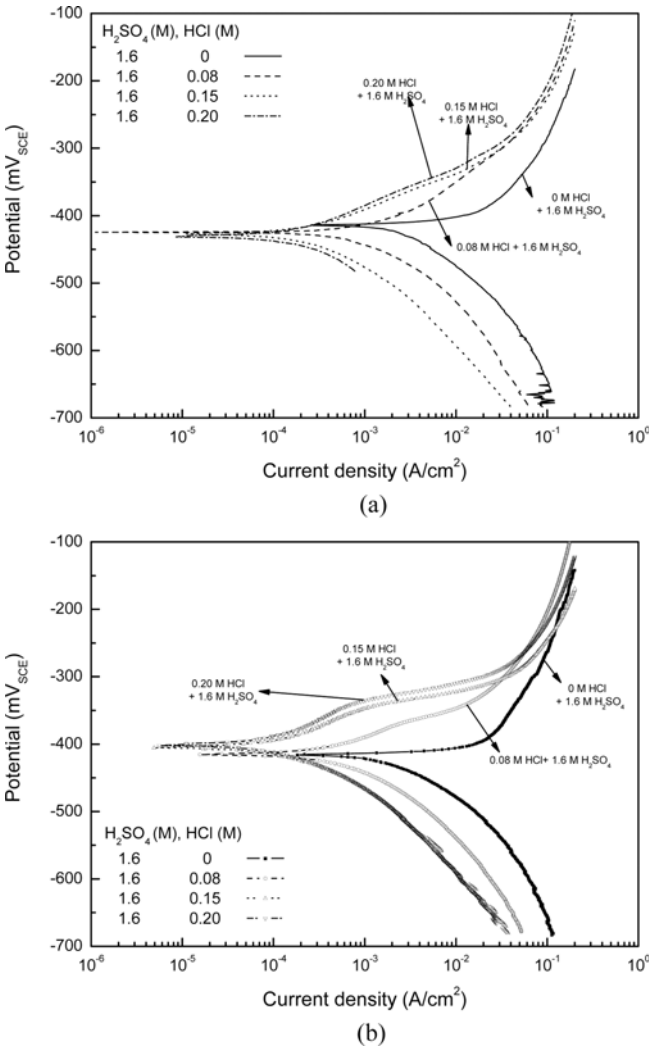

Fig. 2. Potentiodynamic polarization curves of specimens after the stable open-circuit potential (OCP) of the specimen was obtained (for about 20 min), and after 6 h of immersion in a dilute sulfuric acid solution with various concentrations of hydrochloric acid. (a) initial immersion and (b) 6 h immersion.

$$\text{Corrosion rate (mm/y)} = \frac{3.16 \times 10^2 i_{corr} M}{zF\rho} \quad (2)$$

where i_{corr} is the corrosion current density ($\mu A/cm^2$), M is the molar mass of the metal (g/mol), z is the number of electrons transferred per metal atom, F is Faraday's constant, and ρ is the density of the metal (g/cm^3).

In general, the protection efficiency is directly proportional to the amount of inhibitor adsorbed or to the degree surface coverage. The protection efficiency (P_i) can be calculated using potentiodynamic polarization tests results according to the following Eq. [21-25]:

$$p_i = \frac{i^o_{corr} - i_{corr}}{i^o_{corr}} \quad (3)$$

where i^o_{corr} and i_{corr} are the corrosion current densities with-

Table 1. Results of the potentiodynamic polarization test

Test solution	1.6 M H_2SO_4		0.08 M HCl + 1.6 M H_2SO_4		0.15 M HCl + 1.6 M H_2SO_4		0.20 M HCl + 1.6 M H_2SO_4	
	Initial	After 6 h	Initial	After 6 h	Initial	After 6 h	Initial	After 6 h
E_{corr} (mV)	-414.6	-411.2	-424.4	-415.1	-426.7	-404.5	-425.9	-401.1
I_{corr} ($\mu A/cm^2$)	5813	6218	1707	673.5	345.6	216.6	242.2	202.3
CR (mm/y)	67.58	72.28	19.84	7.83	4.02	2.52	2.82	2.35
P_i (%)	-	-	70.64	89.17	94.05	96.51	95.83	96.75

out and with hydrochloric acid, respectively.

Table 1 summarizes the potentiodynamic polarization data, highlighting the beneficial effects of chloride ions. The protection efficiency was increased due to the addition of hydrochloric acid, confirming that protective corrosion production layers were formed by the addition of chloride ions.

3.3. Potentiostatic polarization tests

As shown in Fig. 2, the anodic current density from 0 V_{OCP} to 0.1 V_{OCP} was reduced due to the addition of hydrochloric acid, confirming the improved corrosion resistance by the addition of chloride ions. The relative surface stability of the specimens was evaluated by the potentiostatic test based on the data from the polarization curves in Fig. 2, which corresponds to the enrichment of the protective film. Figure 3 shows the results of the potentiostatic test performed at a constant potential of -0.35 V_{SCE} for 6 h. The current density increased upon immersion due to metal dissolution, and then reached a steady state during the test time. This suggests that the decrease in current density is related to a lower anodic dissolution with increasing hydrochloric acid concentration, which is in agreement with the polarization test results. In particular, in the case of the 0.15 M HCl+H_2SO_4 solution, the noise phenomena in potentiostatic polarization curve represent the instability of film. However, the current density of 0.15 M HCl+H_2SO_4 solution was lower than that of 0.00, 0.08 M HCl+H_2SO_4 solution, confirming the improved corrosion resistance.

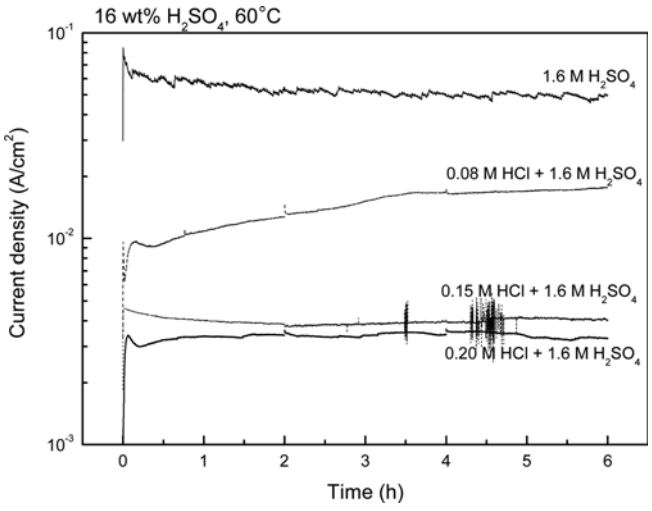

Fig. 3. Current variation with time at the potential of -0.35 V_{SCE} for 6 hours in a dilute sulfuric acid solution with various concentrations of hydrochloric acid.

3.4. Variation of corrosion rate with time

To confirm the potentiodynamic and potentiostatic polarization results and obtain a better understanding of the effect of chloride ions on the corrosion behavior of low-alloy steel, EIS measurements were carried out in a dilute sulfuric acid solution with various concentrations of hydrochloric acid every 1 h until 6 h. Figure 4 shows the Nyquist plot obtained for the steels with different immersion times under the open-circuit potential. The Nyquist diagrams consisted of a capacitive semicircle in the high-medium frequency range and an inductive loop in the low frequency range. The capacitive semicircle characterizes the active state of the interface when the steel is exposed to the sulfuric acid solution. The inductive loop observed in Fig. 4(a), which occurs at low frequency, is attributed to the increase of corrosion rate during measurement [25-29]. The inductive signal present at the low frequency disappears and the amplitude of the capacitive semicircle increases with the addition of chloride ions, as shown in Fig. 4(b), (c), and (d) [30-32].

Table 2 summarizes the best fitting values of the capacitive semicircle, these impedance results can be fitted to the circuit model seen in Fig. 5. The fit consists of the following elements: R_s, which is the solution resistance of the test electrolyte between the working and reference electrodes, and C_{rust} is the rust capacitance generated by the dielectric properties of the rust. R_{ct} is the charge-transfer resistance of the substrate to corrosion. Constant phase elements (CPEs) were used for data fitting to allow for depressed semicircles. L_1 and L_2 are the inductance of solution and partial protective film, respectively. The capacitances were replaced with CPEs to improve the quality of the fit. The total polarization resistance is equal to R_{ct} [29-30].

The corrosion current density was determined using the Tafel extrapolation method. The polarization resistance, R_P, is inversely proportional to the corrosion current density according to the following equation [10]:

$$R_P = \frac{\beta_a \beta_c}{2.3 i_{corr}(\beta_a + \beta_c)} \quad (4)$$

where β_a and β_c are the anodic and cathodic Tafel slopes,

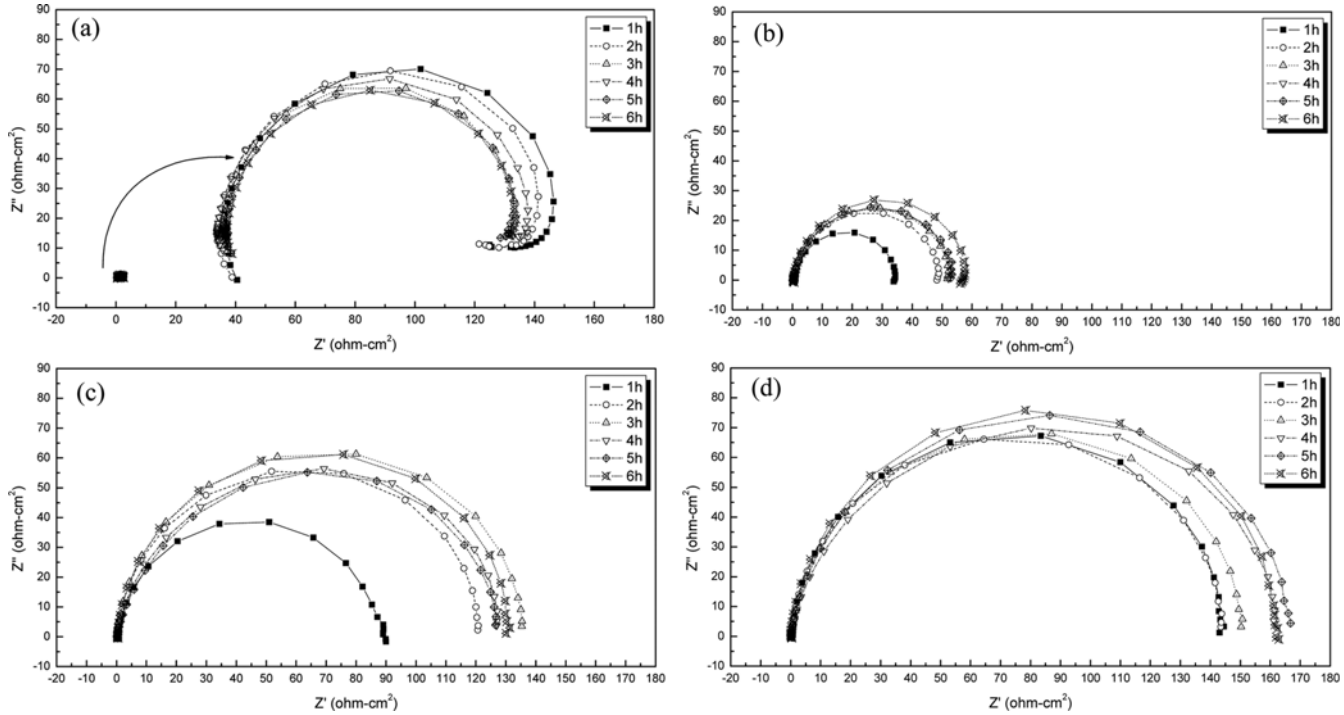

Fig. 4. Nyquist plots as a function of time: (a) 1.6 M H_2SO_4, (b) 0.08 M HCl + 1.6 M H_2SO_4, (c) 0.15 M HCl + 1.6 M H_2SO_4, and (d) 0.20 M HCl + 1.6 M H_2SO_4.

Table 2. Impedance parameters of specimens at various immersion times (a) 0 M HCl and (b) 0.08, 0.15, 0.20 M HCl

Test solution	t (h)	L_1 (H/cm^2)	R_s (Ω/cm^2)	CPE1		R_{ct} (Ω/cm^2)	R_L (Ω/cm^2)	L_2 (H/cm^2)	I_{corr} ($\mu A/cm^2$)	Corrosion rate (mm/y)
				C_{rusr} (mF/cm^2)	n (0~1)					
+ 1.6 M H_2SO_4	1	5.3×10^{-7}	0.527	0.558	1	2.18	11.76	2.00	9967.5	115.63
	2	5.2×10^{-7}	0.484	0.657	1	2.13	11.33	2.25	10211	118.46
	3	2.0×10^{-7}	0.501	0.615	1	1.98	55.78	21.2	10963	127.18
	4	1.9×10^{-7}	0.471	0.660	1	2.08	45.23	42.8	10457	121.30
	5	2.3×10^{-7}	0.522	0.647	1	1.94	35.40	20.0	11217	130.13
	6	2.3×10^{-6}	0.529	0.804	1	1.93	49.02	45.8	11246	130.47

Test solution	t (h)	L_1 (H/cm^2)	R_s (Ω/cm^2)	CPE1		R_{ct} (Ω/cm^2)	I_{corr} ($\mu A/cm^2$)	Corrosion rate (mm/y)
				C_{rusr} (mF/cm^2)	n (0~1)			
0.08 M HCl + 1.6 M H_2SO_4	1	5.6×10^{-7}	0.567	0.734	0.949	34.23	635.09	7.368
	2	4.9×10^{-7}	0.298	0.754	0.950	48.83	445.20	5.165
	3	5.5×10^{-7}	0.564	0.801	0.950	52.16	416.78	4.835
	4	5.4×10^{-7}	0.620	0.900	0.938	53.12	409.25	4.748
	5	5.2×10^{-7}	0.636	0.946	0.939	53.47	406.57	4.717
	6	1.5×10^{-6}	0.302	0.936	0.922	58.26	373.14	4.329
0.15 M HCl + 1.6 M H_2SO_4	1	1.4×10^{-6}	0.431	0.128	0.939	92.23	235.71	2.734
	2	6.2×10^{-7}	0.232	0.274	0.962	120.8	179.96	2.088
	3	6.3×10^{-7}	0.255	0.275	0.952	135.6	160.32	1.860
	4	6.3×10^{-7}	0.287	0.340	0.924	127.8	170.10	1.973
	5	6.2×10^{-7}	0.306	0.406	0.901	127.7	170.24	1.975
	6	8.8×10^{-7}	0.351	0.405	0.961	131.2	165.70	1.922
0.20 M HCl + 1.6 M H_2SO_4	1	9.7×10^{-7}	0.386	0.168	0.961	144.3	150.65	1.748
	2	4.9×10^{-7}	0.298	0.232	0.951	144.4	150.55	1.746
	3	5.0×10^{-7}	0.260	0.270	0.937	151.4	143.59	1.666
	4	5.1×10^{-7}	0.281	0.316	0.911	162.4	133.86	1.553
	5	5.0×10^{-7}	0.279	0.284	0.926	167.2	130.02	1.508
	6	1.2×10^{-6}	0.228	0.153	0.998	159.5	136.30	1.581

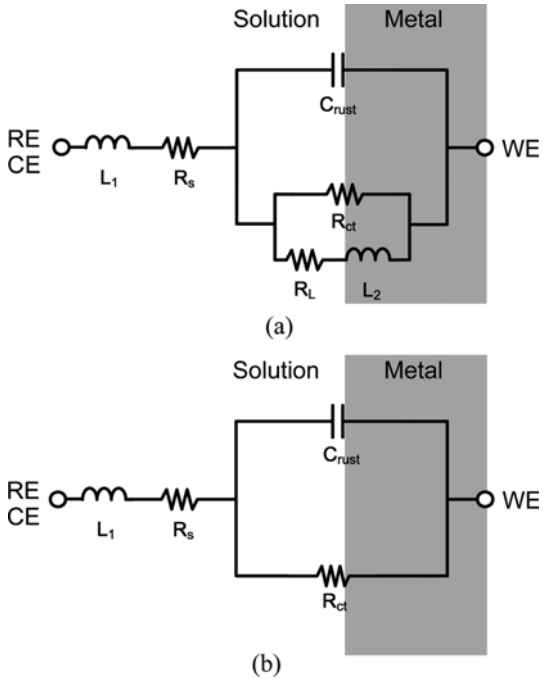

Fig. 5. Equivalent circuit for fitting the EIS data; WE and RE are the working and reference electrodes, respectively: (a) 1.6 M H_2SO_4 and (b) 0.08, 0.15, 0.20 M HCl + 1.6 M H_2SO_4.

respectively, and i_{corr} is the corrosion current density of each specimen.

The corrosion current density of the steel was calculated using Eq. (4). Similarly, the corrosion rate of the steel was calculated from the EIS measurements using Eq. (2), and the results are presented in Table 2 and Fig. 6.

The corrosion rate of the steel in 1.6 M H_2SO_4 decreased with increasing hydrochloric acid. The corrosion rate increased with immersion time in the absence of hydrochloric acid, but it decreased with immersion time with the addition of hydrochloric acid. The decrease of corrosion rate with immersion time indicated that a protective film was formed on the corrosion production layer by adding chloride ions.

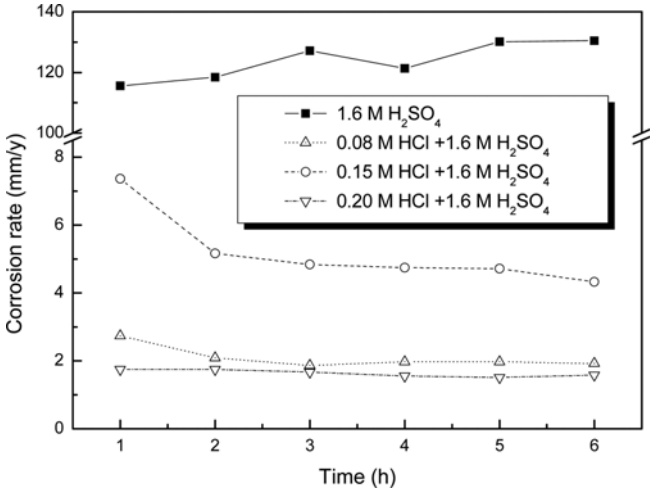

Fig. 6. Corrosion rates determined by EIS as a function of time.

3.5. Surface analyses

The electrochemical and chemical measurements only supported the final conclusion regarding the effect of hydrochloric acid addition on the corrosion resistance of steels. Surface analysis was carried out to determine the mechanism of the effect of chloride ions on the corrosion behavior of low-alloy steels in a dilute sulfuric acid solution. Figure 7 shows SEM images of the corroded surfaces after 6 h immersion. The surface of the steel that was not exposed to hydrochloric acid was rough and uneven compared to the steels that were exposed.

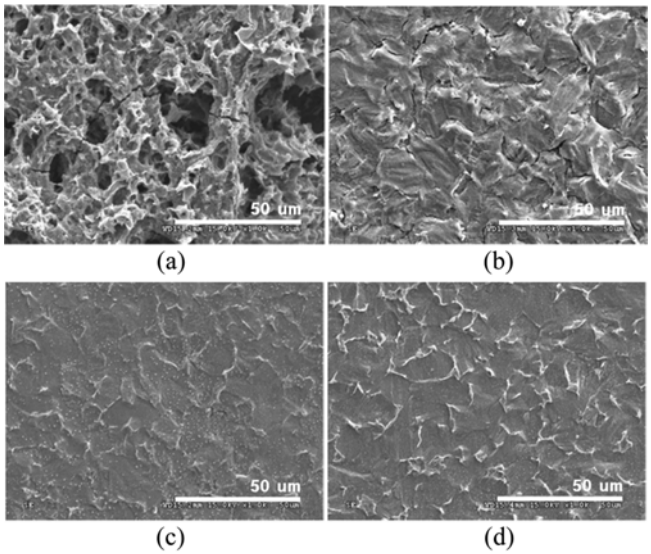

Fig. 7. SEM image of specimens after 6 h of immersion: (a) 1.6 M H_2SO_4, (b) 0.08 M HCl + 1.6 M H_2SO_4, (c) 0.15 M HCl + 1.6 M H_2SO_4, and (d) 0.20 M HCl + 1.6 M H_2SO_4.

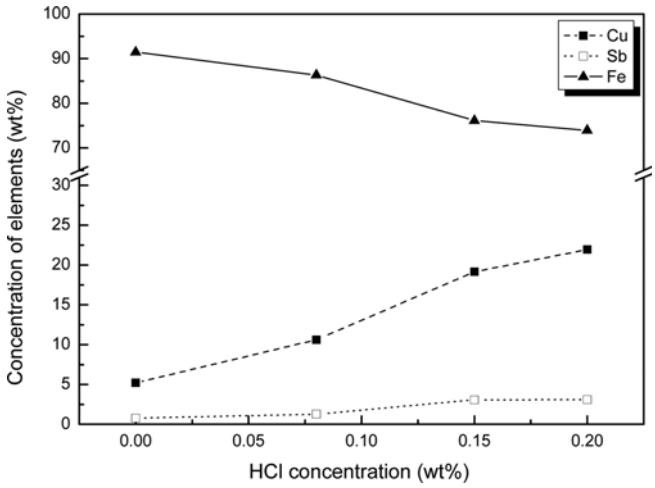

Fig. 8. EDS quantitative analysis of the corroded surfaces after 6 h of immersion in a dilute sulfuric acid solution with various concentrations of hydrochloric acid.

Hence, the corrosion damage to the steels decreased with increasing hydrochloric acid concentration, indicating that chloride ion addition retards the corrosion process. EDS analysis was performed to determine the concentration of the alloying element in the corrosion production layer after 6 h immersion. Figure 8 shows the EDS quantitative analysis of the corroded surfaces after 6 h. These results indicate that dilute Cu and Sb increased in the corrosion production layer with increasing hydrochloric acid.

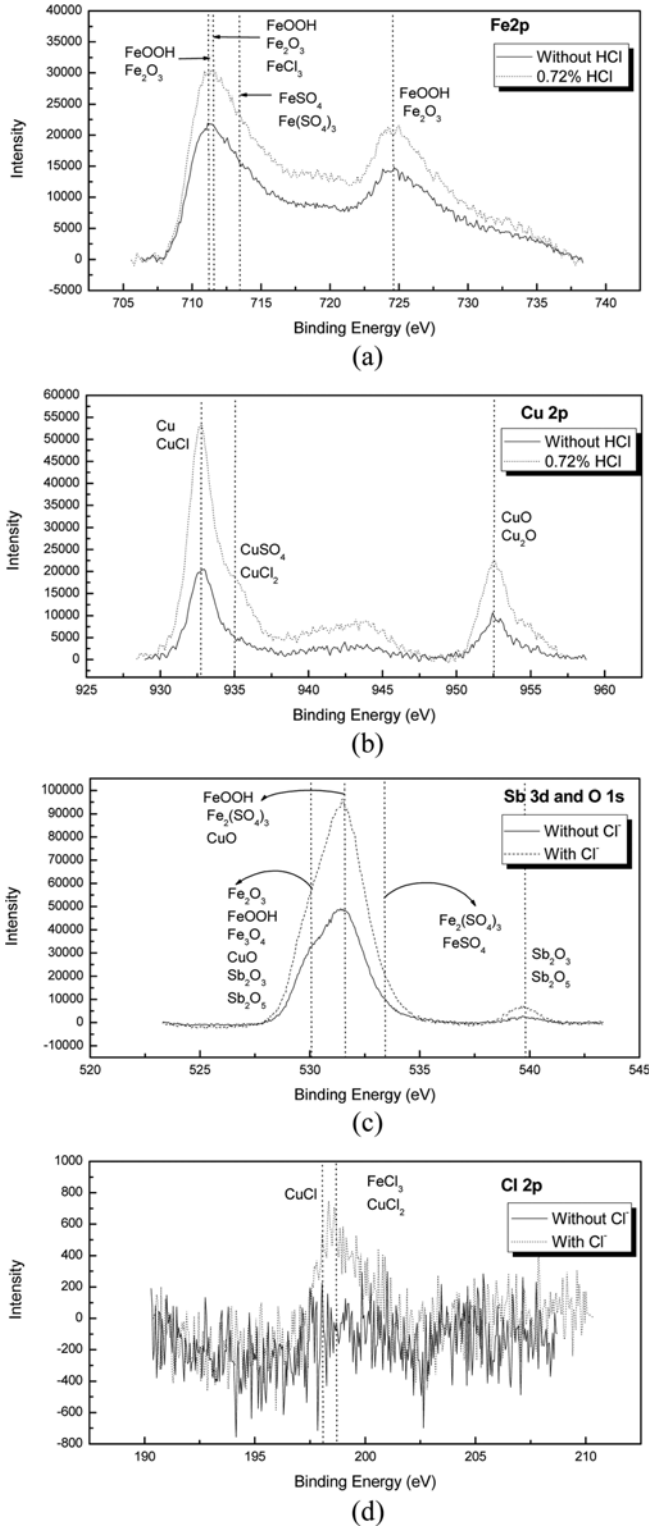

Fig. 9. XPS peak analysis for the surface products of the steels after 6 h of immersion: (a) Fe, (b) Cu, (c) Sb, and O (d) Cl.

The XPS results were examined to determine the chemical composition of the surface layer. Figure 9 shows the XPS spectra of all elements in the surface layers. Fe, Cu, Sb, O, and Cl are essential for the corrosion process on the steel surfaces. Fe_3O_4, Fe_2O_3, FeOOH, $FeSO_4$, $Fe_2(SO_4)_3$, CuO, Cu_2O, $CuSO_4$, CuCl, $CuCl_2$, and Sb_2O_3, Sb_2O_5 were detected on the surface of the specimens shown in the XPS spectra [1,30]. The tendency of steels to form Fe/Cu/Sb oxides, Fe/Cu sulphide and sulphate compounds, and Cu chloride increases with the addition of hydrochloric acid.

4. DISCUSSION

The formation of a metallic, Cu-enriched layer on the surface of steels containing Cu and Sb can be explained by the preferential dissolution and re-deposition process in sulfuric acid solutions with and without hydrochloric acid. According to the E-pH-diagram (Pourbaix diagrams) for Fe and Cu, the dissolution of Fe (as Fe^{2+}) into the acid solution occurs at the potential above -886 mV_{SCE}, whereas Cu dissolution (as Cu^{2+}) occurs at the potential above -97 mV_{SCE}, assuming an activity of 10^{-6} for all dissolved ions [12,25,33]. In an acid solution that contains dissolved oxygen, both Fe and Cu dissolve, but the dissolved Cu is re-deposited as a precipitate of re-crystallized Cu and Cu oxides [30,34]. Especially, the copper deposition performance was increased with increasing hydrochloric acid by adsorbed complex salts.

As a rule, copper exists in valency states +1 and +2. In early nomenclature, monovalent compounds were referred to as cuprous, and divalent compounds were referred to as cupric [23]. Both of these are involved in copper deposition. The copper deposition in acidic sulphate solution is generally accepted to occur through two consecutive reactions:

$$Cu^{2+} + e^- \rightarrow Cu^+ \text{ (RLS, slow)} \quad (5)$$

$$Cu^+ + e^- \rightarrow Cu \text{ (fast)} \quad (6)$$

The first reaction is the rate-limiting step (RLS). In order to control the deposition kinetics, microstructure, and morphology of the electrodeposited films, the addition of several additives to the electrolyte is necessary. The chloride ion has a catalytic action on copper deposition and a definite influence on the structure, orientation and dynamics of surface steps. The chloride ion accelerates the reduction of copper through the formation at the electrode surface of a CuCl monolayer, generated by the following reaction [34-37]:

$$Cu^{2+} + Cl^-_{ads} + e^- \rightarrow CuCl_{ads} \quad (7)$$

which is then reduced through reaction (7):

$$CuCl_{ads} + e^- \rightarrow Cu + Cl^- \quad (8)$$

Therefore, under chloride conditions, the Cu-enriched corrosion production layer is rapidly formed on the surface by the Cl^- catalyst reactions. $CuCl_{ads}$ previously formed on the surface reacts with electrons from the substrate Fe dissolving reaction. Because CuCl crystals are easily consumed by reaction (8), few CuCl crystals will be found on the surface corrosion production layer [34-37]. The selective dissolution and re-deposition process will repeat until the Cu-enriched layer is stabilized [30]. Therefore, the decrease in corrosion rate with increasing chloride ions is caused by an accelerated rate-limiting step of the copper deposition.

Chloride ions are among the most common additives, and understanding their influence on the deposition process is of central importance for understanding the combined effect of all the other additives [34-43]. The reduction potential for antimony in chloride media lies close to the reduction potential of Cu(I). Therefore, the effect of antimony on copper deposition from chloride electrolytes is more significant than that in the absence of chloride electrolytes [44-45]. As a rule, antimony exists in valency state +3. In early nomenclature, its trivalent compounds were referred to as antimonous [35].

The Cu deposition process by an adsorbed complex salt of low-alloy steel containing Cu and Sb in sulfuric acid with hydrochloric acid is shown in Fig. 10. The process is split into two steps: (1) The adsorbate under the coexistence of Sb(III) and Cu(I) chloride is a complex salt containing cuprous and antimonous chlorides. The adsorption increases with acidic environments when the solution contains both Cu and Sb. (2) The discharge of cuprous ions in the adsorbed complex salt releases antimonious ions and chloride, and then forms a new layer of the complex salt with cuprous ions from the solution. This newly formed complex salt is readsorbed on the surface [44-45]. The adsorption of Sb(III) and Cu(I) chloride species at the surface increases the precipitation of re-crystallized Cu. By considering that CuCl rather than Cu^+ is the electrochemically active species upon the electrodeposition of copper from chloride electrolytes, a salt containing Cu, Sb, and chloride is the proper electrochemically active species of Cu electrodeposition when Sb is involved. Therefore, the decrease in corrosion rate with increasing chloride ions of low-alloy steel containing copper and antimony is caused by an accelerated reaction of copper deposition through the adsorbed complex salt, Sb(III), and Cu(I) chloride species. Especially, at relatively high potential the structure of the anodic curves (Fig. 2) is changed in presence of Cl^- showing the variation in the curvature because of the increased copper deposition through the adsorbed complex salt, Sb(III), and Cu(I) chloride species.

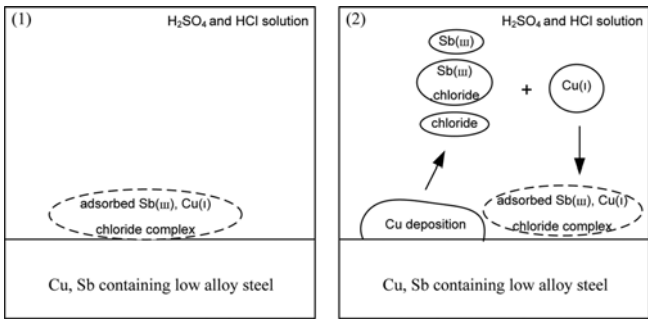

Fig. 10. Schematic diagrams of the Cu deposition by adsorbed complex salt of low-alloy steel containing Cu and Sb in sulfuric acid with hydrochloric acid.

The Cu-enriched layer formed by complex salt, Sb(III) and Cu(I) chloride species, as well as Cu, Sb, and Fe compounds on the surface of the steel containing Cu and Sb contributes to the improvement of corrosion resistance in sulfuric acid solutions with hydrochloric acid added [9]. Because the Cu alloying element is less soluble than Fe, the amount of insoluble oxide in Cu-containing steel was larger than the amount of dissolved oxides in Cu-free steel. This process reduces the level of corrosion damage significantly. Accordingly, Cu-containing steels had more of the protective thick corrosion production layer than Cu-free steel due to the formation of Cu oxides [46]. Sb_2O_5 is the thermodynamically stable form of antimony in the presence of oxygen. Under strongly oxidizing conditions in very acidic solutions, Sb_2O_3 is oxidized to Sb_2O_5. The presence of Sb_2O_5 on the surface of the Sb-containing steels further inhibited the anodic reactions, thereby decreasing the corrosion rate [33,47]. Iron oxyhydroxides (FeOOH) should be formed on the surface of steel upon exposure to the environment due to Fe^{2+}/Fe having the lowest reduction potential compared to other elements. FeOOH is formed by galvanic corrosion of the dissolution oxygen and hydrolysis to $Fe(OH)_3$, which is positively charged and in an colloidal form, and then electrophoretically deposited as FeOOH onto the Cu matrix. Moreover, iron products with other elements incorporated help compact the rust. Although $Fe_2(SO_4)_3$ was detected in all of the specimens, its effect on the corrosion resistance of the low-alloy steels was not confirmed [30,48,49]. Overall, protective metal oxides of alloying elements, such as Cu, Sb, and Fe oxides, increase the corrosion resistance of low-alloy steel in a sulfuric acid solution.

5. CONCLUSIONS

Weight loss measurements and AC and DC electrochemical methods have indicated that the corrosion resistance increases by increasing the addition of hydrochloric acid. Surface analyses (SEM, EDS and XPS) of the corroded surfaces after the immersion test indicated that the tendency of steels to form Fe/Cu/Sb oxides, Fe/Cu sulphide and sulphate compounds, and Cu chloride increases with the addition of chloride ions. The corrosion resistance was improved by Cu/Sb oxide and Fe compounds as a result of the interaction of FeOOH with

Cu. Furthermore, the corrosion resistance was improved by the Cu-enriched layer, in which chloride ions are an accelerator for cupric ion reduction during copper deposition. Cuprous and antimonious chloride species are complex salts for cuprous ions adsorbed on the surface during copper deposition.

ACKNOWLEDGEMENT

This research was supported by the Basic Science Research Program through the National Research Foundation of Korea (NRF), funded by the Ministry of Education, Science and Technology (2010-0022972).

REFERENCES

1. D. P. Le, W. S. Ji, and J. G. Kim, *Corros. Sci.* **50**, 1195 (2008).
2. S.-A. Park, J.-G. Kim, B.-H. Lee, and J.-B. Yoon, *Korean J. Met. Mater.* **52**, 837 (2014).
3. S. A. Park, S. H. Lee, and J. G. Kim, *Met. Mater. Int.* **18**, 957 (2012).
4. M. J. Kim, S. H. Lee, J. G. Kim, and J. B. Yoon, *Corrosion* **66**, 1250051 (2010).
5. S. A. Park, W. S. Ji, and J. G. Kim, *Int. J. Electrochem. Sci.* **8**, 7498 (2013).
6. S. A. Park, J. G. Kim, and J. B. Yoon, *Corrosion* **70**, 196 (2014).
7. J. Okamoto, A. Usami, A. Soeno, H. Mimura, and T. Ishitsuka, *Nippon Steel Tech. Rep.* **90**, 98 (2004).
8. J. Okamoto, A. Usami, and H. Mimura, *Nippon Steel Tech. Rep.* **87**, 46 (2003).
9. A. Usami, M. Okushima, S. Sakamoto, S. Nishimura, T. Kusunoki, and K. Kojima, *Nippon Steel Tech. Rep.* **90**, 25 (2004).
10. D. A. Jones, *Principles and Prevention of Corrosion, 2nd ed.,* pp.31-148, Prentice Hall, New Jersey (1996).
11. T. V. Shibaeva, V. K. Laurinavichyute, G. A. Tsirlina, A. M. Arsenkin, and K. V. Grigorovich, *Corros. Sci.* **80**, 299 (2014).
12. B. Lin, R. Hu, C. Ye, Y. Li, and C. Lin, *Electrochim. Acta* **55**, 6542 (2010).
13. W. S. Li and J. L. Luo, *Corros. Sci.* **44**, 1695 (2002).
14. B. Jegdic, D. M. Drazic, and J. P. Popic, *Corros. Sci.* **50**, 1235 (2008).
15. L. Vracar and D. M. Drazic, *J. Electrochem. Soc.* **110**, 703 (1963).
16. V. J. Drazic, D. M. Drazic, and V. Jevtic, *J. Serb. Chem. Soc.* **52**, 711 (1987).
17. ASTM G 1-90, *Standard Practice for Preparing, Cleaning, and Evaluating Corrosion Test Specimens*, pp.16-23, Annual Book of ASTM Standards, ASTM, West Conshohocken, PA (2002).
18. ASTM G 31-72, *Standard Practice for Laboratory Immersion Corrosion Testing of Metals,* pp.101-108, Annual Book of ASTM Standards, ASTM, West Conshohocken, PA (2002).
19. M. I. Barrena, J. M. Gómez de Salazar, J. M. Vázquez, I. García-Cano, and J. M. Guilemany, *Met. Mater. Int.* **20**, 613 (2014).
20. N. D. Nam, D. Y. Lee, J. G. Kim, and N. J. Park, *Met. Mater. Int.* **20**, 469 (2014).
21. S. H. Lee, W. K. Oh, and J. G. Kim, *Prog. Org. Coat.* **76**, 778 (2013).
22. M. Gojic, *Corros. Sci.* **43**, 919 (2013).
23. B. G. Ateya, B. E. El-Anadouli, and M. El-Nizmay, *Corros. Sci.* **24**, 509 (1984).
24. B. Dus and Z. Szklarska-Smialowska, *Corrosion* **25**, 69 (1969).
25. A. Frignani, M. Tassinari, and G. Trabanelli, *Electrochim. Acta* **34**, 1259 (1989).
26. G. A. Zhang and Y. F. Cheng, *Corros. Sci.* **51**, 87 (2009).
27. Macdonald, *J. Electrochem. Soc.* **125**, 2062 (1978).
28. X. Guo, H. Imaizumi, and K. Katoh, *J. Electroanal. Chem.* **383**, 99 (1995).
29. K. H. Kim, S. H. Lee, N. D. Nam, and J. G. Kim, *Corros. Sci.* **53**, 3576 (2011).
30. J. H. Hong, S. H. Lee, J. G. Kim, and J. B. Yoon, *Corros. Sci.* **32**, 174 (2012).
31. F. Farelas, M. Galicia, B. Brown, S. Nesic, and H. Castaneda, *Corros. Sci.* **52**, 509 (2010).
32. G. Moretti, F. Guidi, and G. Grion, *Corros. Sci.* **46**, 387 (2004).
33. Marcel Pourbaix, *Atlas of Electrochemical Equilibria in Aqueous Solution*, pp.307-392, NACE , Houston (1974).
34. W. P. Dow and H. S. Huang, *J. Electrochem. Soc.* **152**, C67 (2005).
35. W. P. Dow, H. S. Huang, M. Y. Yen, and H. H. Chen, *J. Electrochem. Soc.* **152**, C77 (2005).
36. D. M. Soares, S. Wasle, K. G. Weil, and K. Doblhofer, *J. Electroanal. Chem.* **532**, 353 (2002).
37. D. P. Barkey and F. Oberholtzer, Q. Wu, *J. Electrochem. Soc.* **145**, 590 (1998).
38. M. Tan and J. N. Harb, *J. Electrochem. Soc.* **150**, C420 (2003).
39. D. Stoychev and C. Tsvetanov, *J. Appl. Electrochem.* **26**, 741 (1996).
40. T. Kekeri and M. Isshiki, *J. Appl. Electrochem.* **27**, 982 (1997).
41. H. P. Lee, K. Nobe, and A. J. Pearlstein, *J. Electrochem. Soc.* **132**, 1031 (1985).
42. A. J. Pearlstein, H. P. Lee, and K. Nobe, *J. Electrochem. Soc.* **132**, 2159 (1985).
43. T. P. Moffat, J. E. Bonevich, W. H. Huber, A. Stanishevsky, and D. R. Kelly, *J. Electrochem. Soc.* **147**, 4524 (2000).
44. H. K. Lin and X. Wu, *Metall. Mater. Trans. B* **27B**, 157 (1996).
45. H. K. Lin, X. Wu, and P. D. Rao, *J. Appl. Electrochem.* **24**, 758 (1994).
46. Y. S. Choi, J. J. Shim, and J. G. Kim, *J. Alloys Compd.* **391**, 162 (2005).
47. A. L. Pitman, M. Pourbaix, and N. de Zoubov, *J. Electrochem. Soc.* **104**, 594 (1957).
48. N. D. Nam and J. G. Kim, *Corros. Sci.* **52**, 14 (2010).
49. R. F. North and M. J. Pryor, *Corros. Sci.* **9**, 509 (1969).